Hetero-deformation-induced (HDI) plasticity induces simultaneous increase in both yield strength and ductility in a $Fe_{50}Mn_{30}Co_{10}Cr_{10}$ high-entropy alloy

Dong Liu, Jing Wang, Chang Wang, et al.

COLLECTIONS

Paper published as part of the special topic on Metastable High Entropy Alloys

View Online   Export Citation   CrossMark

ARTICLES YOU MAY BE INTERESTED IN

Martensitic transformation in CrCoNi medium-entropy alloy at cryogenic temperature
Applied Physics Letters **119**, 131901 (2021); https://doi.org/10.1063/5.0067268

Metastability engineering of partially recrystallized C-doped non-equiatomic CoCrFeNiMo medium-entropy alloy
Applied Physics Letters **119**, 141901 (2021); https://doi.org/10.1063/5.0065000

Effect of short-range order on the mechanical behaviors of tensile and shear for NiCoFeCr
Applied Physics Letters **119**, 131904 (2021); https://doi.org/10.1063/5.0064420

Hetero-deformation-induced (HDI) plasticity induces simultaneous increase in both yield strength and ductility in a $Fe_{50}Mn_{30}Co_{10}Cr_{10}$ high-entropy alloy

Dong Liu,[1,2] Jing Wang,[1] Chang Wang,[3] Ping Jiang,[1] Fuping Yuan,[1,2] and Xiaolei Wu[1,2,a]   (iD)

AFFILIATIONS

[1]State Key Laboratory of Nonlinear Mechanics, Institute of Mechanics, Chinese Academy of Sciences, Beijing 100190, China
[2]School of Engineering Science, University of Chinese Academy of Sciences, Beijing 100049, China
[3]Special Steel Department, Central Iron and Steel Research Institute, Beijing 100081, China

Note: This paper is part of the APL Special Collection on Metastable High Entropy Alloys.
[a]Author to whom correspondence should be addressed: xlwu@imech.ac.cn

ABSTRACT

Low yield strength is the bottleneck of the face-centered cubic-structured high-entropy alloys (HEAs). Here, the strategy of hetero-deformation-induced (HDI) plasticity is applied by hetero-structuring to induce strengthening and strain hardening for a simultaneous increase in both yield strength and ductility in a $Fe_{50}Mn_{30}Co_{10}Cr_{10}$ HEA. The coarse-grain (CG) microstructure is a dual phase consisting of face-centered cubic (γ) and hexagonal close-packed (ε) phases, along with phase transformation from γ to ε to happen during tensile deformation. The hetero-structure (HS) was designed, besides recrystallized γ and ε, specifically to reserve a part of deformed γ after cold rolling followed by incomplete recrystallization. Yield strength increases from 200 MPa in CG to 760 MPa in HS, while uniform elongation (i.e., ductility) increases from 35% to 38%. The tensile load-unload-reload testing showed the ceaselessly presence of hysteresis loop during each unload-reload cycle. Both the residual plastic strain and HDI stress were measured with tensile strains in both HS and CG, providing solid evidence of the effect of HDI plasticity. To be specific, the HDI stress is found to account for a large proportion of global flow stress in HS as compared to that in CG. It turns out that the HDI plasticity facilitates both HDI strengthening and HDI strain hardening, which play the crucial role in enhancing strength and ductility. The microstructural origin of HDI plasticity in HS was ascribed to plastic incompatibility at hetero-interfaces of among varying grains as evidenced by the evolution of Schmid factor and KAM values as well.

The face-centered cubic (fcc)-structured high-entropy alloy (HEA) has the advantage of large ductility and toughness, but suffers from low yield strength.[1–3] The fcc HEA is observed to plastically deform by the intra-granular dislocation plasticity, similar to that in traditional metallic materials.[1–5] The varying strengthening mechanisms suitable to traditional metallic materials are still able to be applicable in fcc HEAs, e.g., the nano-precipitation[6–8] and solid solution.[9] Yet, the increase in strength always accompanies a dramatic loss in ductility.[2,3,10] This strength-ductility trade-off is, actually, ascribed to a long nerve-wracking paradox between the strengthening and strain hardening closely associated with the intra-granular dislocation behaviors during plastic deformation.[2,3,11,12] To the best of both worlds,

several strategies have been proposed so far. For example, the nano-precipitation is shown to be a successful selection in HEAs,[6–8] but often with a complicated alloying in HEAs.

Recently, hetero-structuring is advocated to enhance ductility especially as an elevated yield strength.[13–24] The hetero-structure (HS) is usually composed of soft and hard grains of varying flow stresses. Upon plastic straining, plastic incompatibility, along with strain gradient, results near the hetero-interfaces where compatible deformation is necessary. As a result, the geometrically necessary dislocations are produced, usually in the form of pile-ups, which will interact later with traditional forest dislocations. This leads to back stress in soft grains and forward stress in hard ones,[13,14] which collectively produce the

hetero-deformation-induced (HDI) stress.[14–17] The HDI stress induces the HDI plasticity. Specifically, the HDI plasticity leads to HDI strain hardening with applied strain to help with retaining ductility.[13] Furthermore, successively yielding in HS is an elasto-plastic co-deformation due to the varying flow stresses in grains.[16] This induces the strengthening effect, causing an increase in yield strength beyond the prediction of the rule-of-mixture.[16,18,25]

In this study, a HS was designed in a quaternary non-equiatomic ratio $Fe_{50}Mn_{30}Co_{10}Cr_{10}$ (at. %) HEA. This HEA itself has been the coarse-grained (CG) hetero-structure already, consisting of dual-phases (DP) of fcc γ-phase and hexagonal close-packed ε-phase.[11] Furthermore, phase transformation from γ to ε happens during tensile deformation. Namely, the transformation-induced plasticity (TRIP) effect is the dominant mechanism for both the plastic deformation and strain hardening.[11] Here, the HS is deliberately designed by cold rolling followed by partial recrystallization annealing. By comparison to CG with recrystallized γ- and ε-grains, HS has the key microstructural feature in retaining a part of deformed γ-phase of high strength, with two purposes. One is to significantly enhance yield strength, while the other is to amplify the microstructural heterogeneity to induce strain hardening for a simultaneous increase in ductility.

The $Fe_{50}Mn_{30}Co_{10}Cr_{10}$ HEA was produced by arc-melting pure elements (all >99.9% purity) and subsequently casting into iron mold of a 150 mm diameter under an argon atmosphere. To ensure homogeneity, ingot was re-melted five times and flipped multiple times. The ingot was multi-directionally hot-forged and hot-rolled at the temperature of 1150 °C to plates of the dimension of $12 \times 80 \times 800$ mm³ and then, vacuum heat-treated for homogenization at 1150 °C for 24 h, followed by rapidly quenching in water. This microstructure is specified as the coarse-grain (CG) counterpart in the present study. The plate was hot rolled and cold rolled with to final thickness of 1 mm. The hetero-structure (HS) was finally obtained by incomplete recrystallization annealing at a temperature of 600 °C for 1 h. Tensile specimens were cut along the rolling direction, with a gauge cross section of 4×1 mm² and 15 mm in length. Tensile testing was performed using MTS 793 machine at room temperature and at a strain rate of 5×10^{-4} s⁻¹. The microstructure was then characterized using the electron backscattered diffraction (EBSD) imaging in a ZEISS Supra 55 scanning electron microscope (SEM) with an EBSD detector before and after tensile straining. Both the Schmid factor and Kernel Average Misorientation (KAM) values were measured near the hetero-interfaces. Foils before and after tensile straining for TEM observations were thinned and polished to 50 μm thick from the sheets, punched to disks of 3 mm in diameter and perforated finally in a twin-jet electro-polishing using a solution of 8 vol. % perchloric acid and 92 vol. % alcohol at the temperature of -25 °C and a voltage of 30 V.

Figure 1 summarizes the microstructural characterization of HS, along with that in CG for comparison. The x-ray spectra indicate dual phases of both γ and ε in both HS and CG, see Fig. 1(a). The initial volume fraction of ε-phase is determined to be, respectively, 13% in HS and 28.6% in CG before tensile testing, which increases to 50.4% and 66.3% after tensile deformation. This indicates that phase transformation from γ to ε happens during tensile deformation in both microstructures.[11] Figures 1(b)–1(d) are, respectively, the EBSD
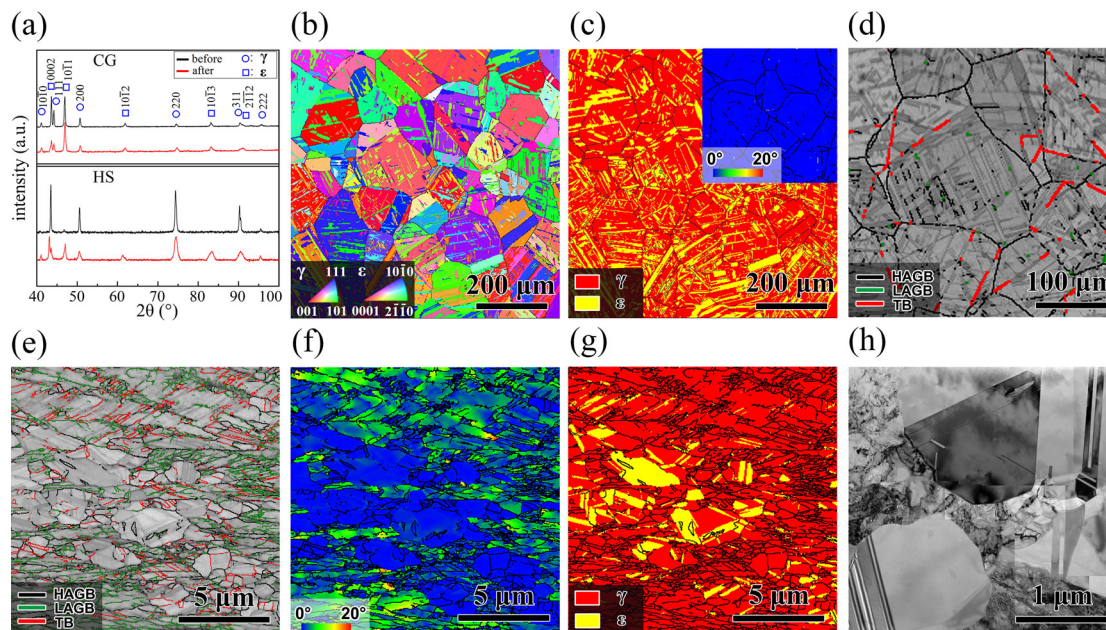

FIG. 1. (a) X-ray spectra of both the hetero-structure (HS) and coarse-grained (CG) counterpart, respectively, before and after tensile deformation in the $Fe_{50}Mn_{30}Co_{10}Cr_{10}$ high-entropy alloy. Both show the face-centered cubic (fcc, γ) and hexagonal close-packed (hcp, ε) dual phase. (b)–(d) EBSD inverse pole figure, phase figure, and close-up view of quality figure in conjunction with grain boundary information, respectively, showing the microstructure in CG after recrystallization. Inset in (c): GROD figure. (e)–(h) Quality figure, GROD figure, phase figure, and TEM micrograph in HS after recrystallization. Note green areas indicating deformed structures retained after incomplete recrystallization in (f). Note the presence of ε-phase in yellow mainly in recrystallized γ-grains in (g). Note deformed γ-grains with dislocation cells of high density in (h), in contrast to fully-recrystallized, dislocation-free γ-grains.

inverse pole figure, phase figure, and close-up view quality figure over-lapped with grain boundary information in CG. The statistical average size is 116.7 μm for γ-grains. It is visible that CG is, essentially, a DP hetero-structure. The ε-phase dispersedly distributes in the interior of γ-grains, see Fig. 1(c). Both γ and ε have large mismatch of flow stresses.[11] Inset in Fig. 1(c) is the Grain Reference Orientation Deviation (GROD) figure, with full screen in blue, i.e., GROD values less than 2. This indicates complete recrystallization in CG. Figures 1(e)–1(g) are the EBSD quality figure, phase figure, and GROD figure, respectively, in HS. To add all together, of important note is that the HS reserves a part of deformation structure, as seen in the GROD figure [Fig. 1(f)]. The areal fraction in green based on the GROD value > 5° is 57%, indicating the deformed structure, which is not fully recrystallized. This is further evidenced by TEM observations, as shown in Fig. 1(h). The deformed γ-grains contain the dislocation cells, with the dislocation of high density at cell boundaries, in contrast to the recrystallized γ-grains of nearly absence of dislocations. The recrystallized γ-grains show a statistic average size of 0.68 μm. This indicates a significant refinement of γ-grains in HS.

Figure 2(a) is the tensile engineering stress–strain ($\sigma_e - \varepsilon_e$) curve. Of interesting note is the simultaneous rise in both yield strength (σ_y) and ductility (i.e., tensile uniform strain, ε_u) in HS as compared to that in CG. Figure 2(b) is the corresponding true stress and true strain curves. Figure 2(c) shows the curves of a strain hardening rate ($\theta = \partial\sigma/\partial\varepsilon$) as a function of true strain, which is normalized by flow stress (σ_f) due to the large discrepancy in σ_y of varying microstructures. Two dashed curves in homogeneous CG of the same HEA with the average grain size of 45 and 4.5 μm, respectively, are also added for comparison.[11] Interestingly, HS shows a distinct evolution in θ as compared to all three CG. To be specific, θ in HS begins a rapid decline, which then slows down with straining, finally along with a much more gradual falloff as applied strain further increases. This is typical of the response of a strain hardening rate in HS mainly due to the effect of HDI plasticity.[16,17]

The interrupted tensile load-unload-reload (LUR) testing was conducted to further evaluate in detail the responses of strain hardening in both HS and CG. Unload strains were selected discretely in order to evaluate the effect of HDI stress (σ_{HDI}) from the onset of yielding to the end of tensile deformation. Figure 3(a) shows two LUR

stress–strain curves. Both σ_{HDI} and residual plastic strain (ε_{rp}), serving as two key parameters to characterize the effect of σ_{HDI} on both the strengthening and strain hardening,[16,17] were calculated. The method to calculate σ_{HDI} can be found in Ref. 26 in which the measured back stress is actually σ_{HDI}. ε_{rp} is characterized by the width of hysteresis loop upon each unloading,[10] see upper panel in Fig. 3(b).

As seen in Fig. 3, the crucial effect of σ_{HDI} is shown and several distinct features are noteworthy. First, hysteresis loop appears during each unload-reload cycle, see close-up view at two unload strains in Fig. 3(b). The presence of hysteresis loop is a definitive sign of σ_{HDI} to take effect during tensile deformation.[16,17] Of special note is the loop, which occurs already at unload strain of 0.6%, see upper panel in Fig. 3(b), which corresponds to plastic strain of ~0.2%, i.e., tensile/compressive strain at which yielding is usually defined. This is the direct evidence for σ_{HDI} to work already during yielding. In other words, the HDI stress will induce strengthening so as to improve yield strength. Furthermore, the larger the unload strain, the larger ε_{rp} will be in both CG and HS, see Fig. 3(c). The larger ε_{rp} upon unloading indicates the onset of compressive yield flow, even though the sample is still under tensile applied loading.[10] In other words, this is an undoubtedly sign for the generation of σ_{HDI}. Moreover, HS shows a larger ε_{rp} than CG during the initial stage of applied strain smaller than 10%, see Fig. 3(c). The large ε_{rp} indicates a strong HDI hardening, which was called back-stress hardening in earlier literature.[13,14]

Second, σ_{HDI} increases continuously as strain increases in both HS and CG, see Fig. 3(d). The ratio of increment in σ_{HDI}, i.e., $\Delta\sigma_{HDI}$ after yielding to that of flow stress, i.e., $\Delta\sigma_f$ is used to characterize the effect of HDI stress on strain hardening, where $\Delta\sigma_{HDI} = \sigma_{HDI} - \sigma_{HDI,0.2}$, $\Delta\sigma_f = \sigma_f - \sigma_{0.2}$, and $\sigma_{HDI,0.2}$, σ_{flow}, and σ_y are σ_{HDI} at yielding, flow stress, and yield stress, respectively. As shown in Fig. 3(e), the ratio is significantly increased in HS as compared to that in CG. Figure 3(f) shows that the strain hardening rate, Θ, by σ_{HDI} is also much higher in HS than that in CG. These results indicate that the HDI hardening is enhanced in HS and plays a primary role in strain hardening during tensile straining.

The microstructures were characterized to ascertain the origin of HDI hardening in both HS and CG during tensile deformation. Figures 4(a)–4(d) and 4(e)–4(h) are EBSD quality figure, phase figure, Schmid factor figure, and KAM value figure, respectively, in HS and
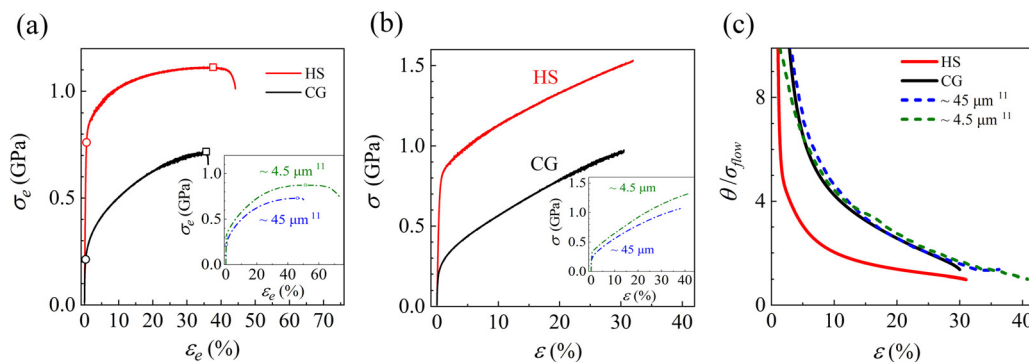

FIG. 2. (a) Tensile engineering stress–strain ($\sigma_e - \varepsilon_e$) curves in HS and CG, respectively. Circle: yield strength. Square: ultimate tensile strength. Inset: $\sigma_e - \varepsilon_e$ curves of homogeneous CG, with the grain sizes of 45 and 4.5 μm in Fe$_{50}$Mn$_{30}$Co$_{10}$Cr$_{10}$ HEA.[11] (b) True stress–strain curves ($\sigma - \varepsilon$). Inset: corresponding $\sigma - \varepsilon$ curves in Fe$_{50}$Mn$_{30}$Co$_{10}$Cr$_{10}$ HEA. (c) Corresponding strain hardening rate ($\theta = \partial\sigma/\partial\varepsilon$) curves, which is normalized by flow stress (σ_f). Two dashed curves: homogeneous CG.[11]
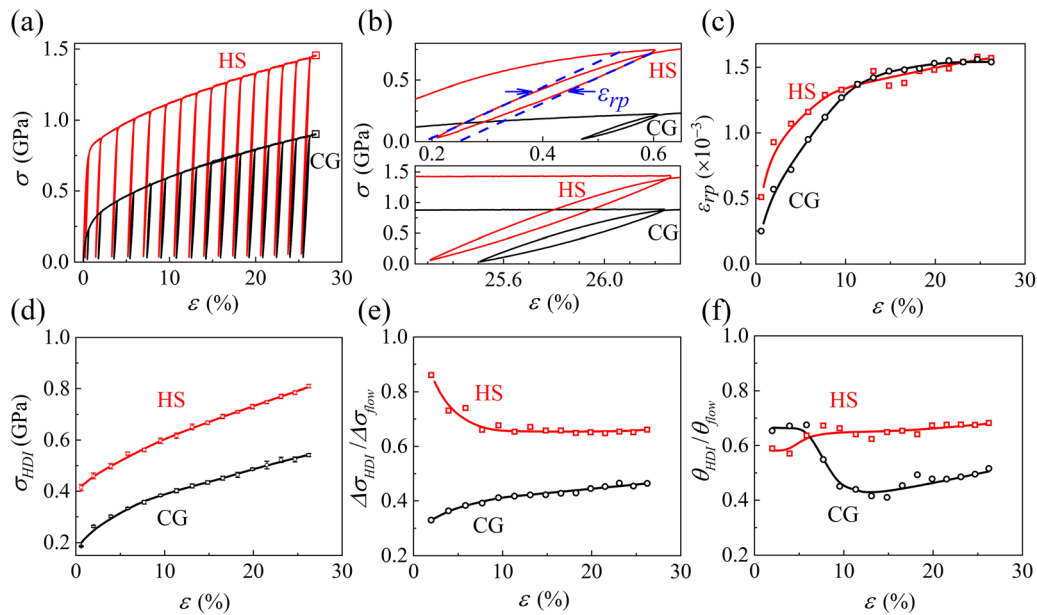
FIG. 3. (a) Tensile load-unload-reload true stress–strain curves in HS and CG, respectively. (b) Close-up view showing hysteresis loop at unload strain of 0.4% (upper panel) and of ~26% (lower panel). (c) and (d) $\varepsilon_{rp}-\varepsilon$ and $\sigma_{HDI}-\varepsilon$ curves. (e) Ratio of increment in σ_{HDI} to that in flow stress after yielding in both HS and CG. (f) Proportion of strain hardening rate by HDI stress to that by flow stress in HS and CG.

CG after tensile deformation. Based on these observations along with the XRD results [Fig. 1(a)], two key microstructural responses are derived. One is phase transformation to happen in both HS and CG, see individual phase figures corresponding to HS and CG, respectively, in Fig. 4, along with an evident increase in volume fraction of the ε-phase. The other is strain accommodation, see KAM value figures in Fig. 4 where the green areas dispersedly distribute, indicating the production of high density GNDs for compatible deformation near hetero-interfaces in both CG and HS, respectively.

To further unveil the origin of HDI stress, both Schmid factor and KAM values were statistically analyzed with the emphasis on the plastic accommodation among varying constituents during tensile deformation. Figures 4(i) and 4(j) show the evolution of Schmid factor in γ- and ε-phases of both HS and CG, respectively, before and after tensile deformation. Only recrystallized γ-grains are considered in HS. Figures 4(k) and 4(l) are corresponding results for KAM values. The change in both Schmid factor and KAM values in both γ- and ε-phases evidences the HDI plasticity in HS and CG. On the one hand, the Schmid factor shows a bi-modal distribution for both γ- and ε-phases in CG, see Fig. 4(i). This indicates plastic deformation to happen in both γ and ε during tensile straining. In contrast, γ-phase in HS also shows a perceptible bi-modal, but rather weak, see Fig. 4(j), along with a shift of average to low values in ε-phase. This indicates that recrystallized γ-grains bear the vast majority of plastic strains during tensile deformation.

On the other hand, the evolution of KAM values further unveils the mechanism behind HDI hardening. In homogeneous CG, KAM values show typical Gaussian distribution in both γ- (upper panel) and ε-phases (lower panel), respectively, prior to (blue curve) and after (red one) tensile deformation, see Fig. 4(k). In contrast, KAM values show different changes in HS, Fig. 4(l). For the γ phase (upper panel),

KAM values (blue curve) show a composite Gaussian distribution before tensile deformation. The narrow distribution at left side, with a clear peak, is mainly ascribed to recrystallized grains, while those of much wide distribution is due to deformed grains, which are remained in HS. After deformation (red curve), the proportion of large KAM values increases, along with the peak obviously moving to the right. This is attributed to back stress, i.e., HDI stress in recrystallized grains where GNDs are produced, leading to an increase in KAM values. Of special note is the decrease in KAM values ranging roughly from 1.5 to 3.5, as indicated by the arrow. This is due to forward stress, i.e., HDI stress but exerting on deformed grains.[15] Forward stress facilitates the dislocations to disentangle especially at hetero-boundaries to lower the density of dislocations in deformed grains.[15,27] As to ε-phase [lower panel in Fig. 4(l)], the KAM value curve (blue) before tensile deformation is also a comprehensive reflection of ε-phases inside recrystallized grains (i.e., narrow Gaussian distribution at the left) and deformed ones (flat at the right). Upon straining, both the increase in the proportion of large KAM values and peak migration to the right are seen, with the similar trend to that of γ-phase mentioned above. The increase in KAM values at varying hetero-boundaries indicates the generation of GNDs, which produce HDI hardening, along with strain accommodation especially between recrystallized grains and deformed ones.

The present HS HEA exhibits a simultaneous increase in both the yield strength and ductility as compared to CG counterpart [Fig. 2(a)]. This synergistic effect is a hallmark of HS materials.[13–25] Specifically, the synergistic effect induces extra strengthening,[10,16,17,25] extra strain hardening,[10,25] and high ductility[13–25] in HS materials. Furthermore, ductility in HS materials is much higher than that measured in standalone deformed microstructure.[16,17] This is mainly ascribed to the HDI stress, which plays a crucial role in sustained
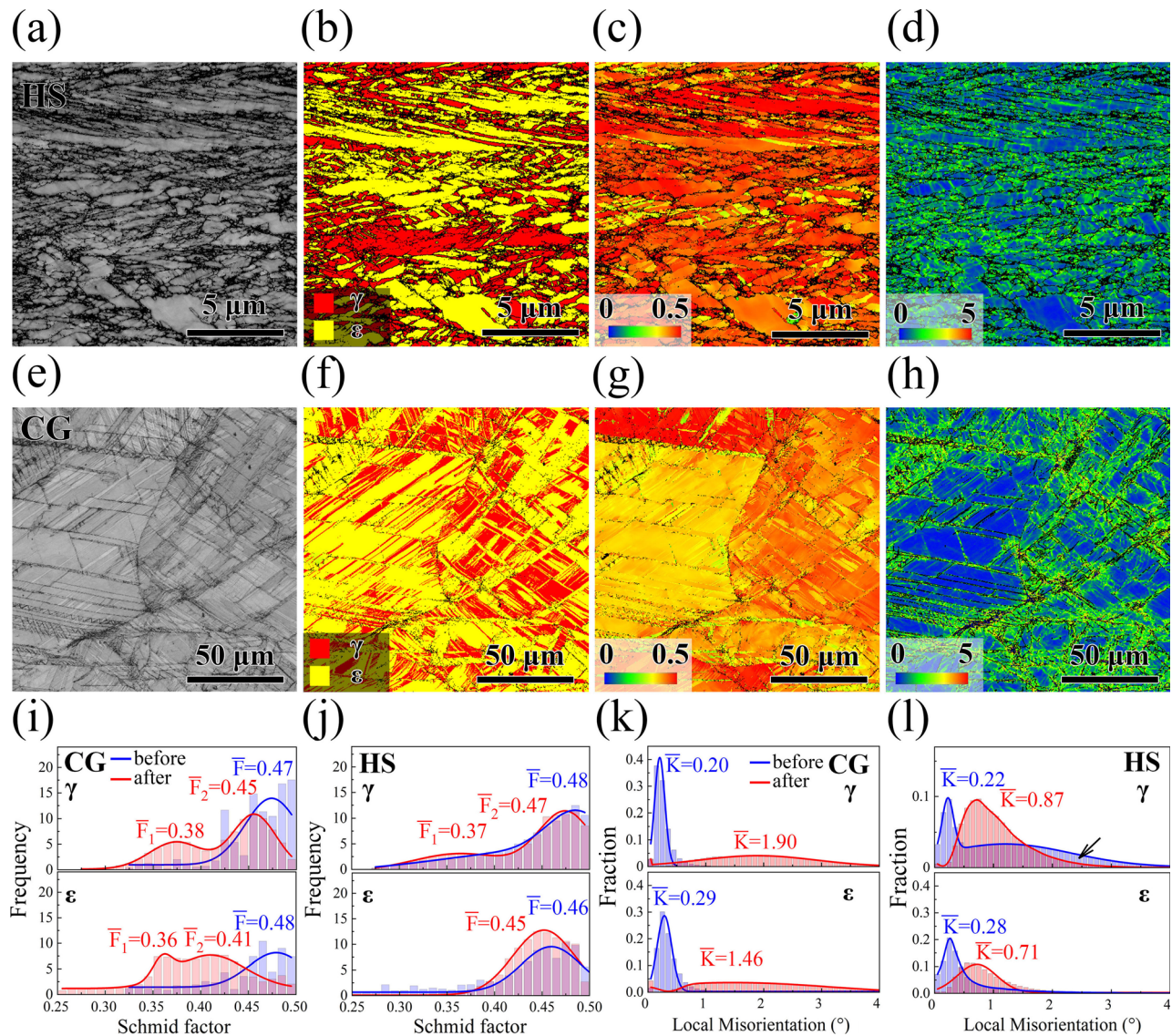
FIG. 4. (a)–(d) and (e)–(h) EBSD quality figure, phase figure, Schmid factor figure, and KAM value figure, respectively, in HS and CG after tensile deformation. (i) and (j) Change in Schmid factor in γ- and ε-phase in CG and HS, respectively, before and after tensile deformation. Only recrystallized γ-phase is analyzed. (k) and (l) Change in KAM values in γ- and ε-phases in CG and HS, respectively, before and after tensile deformation.

plastic deformation, usually called the HDI plasticity. As a result, the trade-off in strength and ductility can be largely alleviated in HS metals.

The increase in yield strength in HS is significant as compared to the CG counterpart [Fig. 2(a)]. Strengthening mechanisms of two kinds play a part. The first lies in reserving a part of deformed γ, with the dislocations of high density inside the interiors. This is one reason for high strength in HS. The second is the grain refinement. The recrystallized γ is within the submicrometer grain scale, smaller than those in traditional CG.[11] This leads to an increase in yield strength according to the Hall–Petch relationship. Last but not least, the HDI stress will induce extra strengthening. Yielding in the present HS

features the elasto-plastic co-deformation.[16,28] This is ascribed to the large discrepancy in yield strength among constituent phases, including deformed and recrystallized γ, and ε-phase. Yielded γ is also constrained such that dislocations inside γ are blocked at hetero-interfaces. This produces a long-range, inter-granular HDI stress to make the dislocation slip difficult. In other words, the HDI stress renders an increased flow stress in γ-grains by the time the whole sample yields. This is the reason for extra strengthening by the HDI stress. Particularly at yielding, the present HS exhibits both large ε_{rp} and σ_{HDI} already, see Figs. 3(b)–3(d), as compared to those in CG. These results lend solid support the presence of extra strengthening effect to enhance yield strength. As for CG, it is expected that extra

strengthening effect is abated due to the absence of deformed γ. Hence, the strengthening effect in HS comes from the rule-of-mixture of constituent phases, i.e., $\Sigma\sigma$, including deformed γ by cold work ($\sigma_{c,w}$), grain refinement ($\sigma_{g,r}$), and initial ε-phase (σ_ε), along with extra strengthening by HDI stress ($\delta\sigma_{HDI}$), as seen in the following equation:

$$\sigma_y = \Sigma\sigma(\sigma_{c,w} + \sigma_{g,r} + \sigma_\varepsilon) + \delta\sigma_{HDI}. \tag{1}$$

The increase in ductility in HS relates still to the HDI stress, which induces extra strain hardening. Both the residual plastic strain and HDI stress increase with applied strain, see Figs. 3(c) and 3(d), indicating the continuously reinforced effect of HDI stress on the sustained plastic deformation and strain hardening. The mechanism of HDI hardening has been revealed in various HS materials.[13–25] The GND pileup is proposed[10,16] in which GNDs are emitted from a Frank–Read source in the grain interior and piled up in front of the hetero-boundary with a GND density gradient.[29] The GND density gradient was later observed near hetero-interfaces,[30] to offset applied stress to impede the emission and slip of dislocations from dislocation sources. As can be seen in Figs. 3, hetero-deformation reigns in HS.[31–33] Two other mechanisms of strain hardening still operate in the present HS. One is the TRIP effect, while the other is forest hardening related to statistically stored dislocations (SSDs) in both recrystallized γ and ε. Therefore, strain hardening in HS can be expressed as

$$\frac{\partial\sigma}{\partial\varepsilon} = \left.\frac{\partial\sigma}{\partial\varepsilon}\right|_{dislos} + \left.\frac{\partial\sigma}{\partial\varepsilon}\right|_{TRIP} + \left.\frac{\partial\sigma}{\partial\varepsilon}\right|_{HDI}. \tag{2}$$

In conclusion, the hetero-structure is deliberately designed in a $Fe_{50}Mn_{30}Co_{10}Cr_{10}$ high-entropy alloy via thermomechanical treatment. To be specific, the deformed fcc phase is preserved due to incomplete recrystallization, along with the grain-refined fcc phase, both contributing to the increment of yield strength as compared to that in the coarse-grained counterpart. Importantly, exactly due to the presence of deformed fcc grains, the hetero-deformation-induced stress is generated. Consequently, the hetero-deformation-induced plasticity contributes to extra strengthening and extra strain hardening, which operate simultaneously, along with the transformation-induced plasticity effect. This causes the synergistic effect in HS. As a result, the trade-off between yield strength and ductility is alleviated largely.

AUTHOR DECLARATIONS

Author Contributions

D.L. and J.W. contribute equally to this work.

DATA AVAILABILITY

The data that support the findings of this study are available within the article.

REFERENCES

[1]B. Gludovatz, A. Hohenwarter, D. Catoor, E. H. Chang, E. P. George, and R. O. Ritchie, Science **345**, 1153–1158 (2014).

[2]E. Ma and X. L. Wu, Nat. Commun. **10**, 5623 (2019).

[3]E. P. George, W. A. Curtin, and C. C. Tasan, Acta Mater. **188**, 435–474 (2020).

[4]S. L. Wei, S. J. Kim, J. Y. Kang, Y. Zhang, Y. J. Zhang, T. Furuhara, E. S. Park, and C. C. Tasan, Nat. Mater. **19**, 1175–1181 (2020).

[5]Z. J. Zhang, M. M. Mao, J. W. Wang, B. Gludovatz, Z. Zhang, S. X. Mao, E. P. George, Q. Yu, and R. O. Ritchie, Nat. Commun. **6**, 10143 (2015).

[6]T. Yang, Y. L. Zhao, Y. Tong, Z. B. Jiao, J. Wei, J. X. Cai, X. D. Han, D. Chen, A. Hu, J. J. Kai, K. Lu, Y. Liu, and C. T. Liu, Science **362**, 933–937 (2018).

[7]Z. F. Lei, X. J. Liu, Y. Wu, H. Wang, S. H. Jiang, S. D. Wang, X. D. Hui, Y. D. Wu, B. Gault, P. Kontis, D. Raabe, L. Gu, Q. H. Zhang, H. W. Chen, H. T. Wang, J. B. Liu, K. An, Q. S. Zeng, T. G. Nieh, and Z. P. Lu, Nature **565**, 546–550 (2019).

[8]Y. Yang, T. Y. Chen, L. Z. Tan, J. D. Poplawsky, K. An, Y. L. Wang, G. D. Samolyuk, K. Littrell, A. R. Lupini, A. Borisevich, and E. P. George, Nature **595**, 245–249 (2021).

[9]Z. M. Li, C. C. Tasan, H. Springer, B. Gault, and D. Raabe, Sci. Rep. **7**, 1–7 (2017).

[10]M. X. Yang, D. S. Yan, F. P. Yuan, P. Jiang, E. Ma, and X. L. Wu, Proc. Natl. Acad. Sci. U. S. A. **115**, 7224–7229 (2018).

[11]Z. M. Li, K. G. Pradeep, Y. Deng, D. Raabe, and C. C. Tasan, Nature **534**, 227–230 (2016).

[12]H. L. Huang, Y. Wu, J. Y. He, H. Wang, X. J. Liu, K. An, W. Wu, and Z. P. Lu, Adv. Mater. **29**, 1701678 (2017).

[13]X. L. Wu, M. X. Yang, F. P. Yuan, G. L. Wu, Y. J. Wei, X. X. Huang, and Y. T. Zhu, Proc. Natl. Acad. Sci. U. S. A. **112**, 14501–14505 (2015).

[14]X. L. Wu and Y. T. Zhu, Mater. Res. Lett. **5**, 527–532 (2017).

[15]Y. T. Zhu and X. L. Wu, Mater. Res. Lett. **7**, 393–398 (2019).

[16]X. L. Wu, Y. T. Zhu, and K. Lu, Scr. Mater. **186**, 321–325 (2020).

[17]X. L. Wu and Y. T. Zhu, MRS Bull. **46**, 244–249 (2021).

[18]R. G. Li, Q. G. Xie, Y. D. Wang, W. J. Liu, M. G. Wang, G. L. Wu, X. W. Li, M. H. Zhang, Z. P. Lu, C. Geng, and T. Zhu, Proc. Natl. Acad. Sci. U. S. A. **115**, 483–488 (2018).

[19]C. E. Slone, J. Miao, E. P. George, and M. J. Mills, Acta Mater. **165**, 496–507 (2019).

[20]S. W. Wu, G. Wang, Q. Wang, Y. D. Jia, J. Yi, Q. J. Zhai, J. B. Liu, B. A. Sun, H. J. Chu, J. Shen, P. K. Liaw, C. T. Liu, and T. Y. Zhang, Acta Mater. **165**, 444–458 (2019).

[21]C. Zhang, C. Y. Zhu, P. H. Cao, X. Wang, F. Ye, K. Kaufmann, L. Casalena, B. E. MacDonald, X. Q. Pan, K. Vecchio, and E. J. Lavernia, Acta Mater. **199**, 602–612 (2020).

[22]K. Ma, Z. Y. Liu, K. Liu, X. G. Chen, B. L. Xiao, and Z. Y. Ma, Carbon **178**, 190 (2021).

[23]R. Geng, Q. L. Zhao, F. Qiu, and Q. C. Jiang, Mater. Res. Lett. **8**, 225–231 (2020).

[24]C. Zhang, C. Y. Zhu, T. Harrington, and K. Vecchio, Scr. Mater. **154**, 78 (2018).

[25]Z. Cheng, H. F. Zhou, Q. H. Lu, H. J. Gao, and L. Lu, Science **362**, eaau1925 (2018).

[26]M. X. Yang, Y. Pan, F. P. Yuan, Y. T. Zhu, and X. L. Wu, Mater. Res. Lett. **4**, 145–151 (2016).

[27]X. L. Wu, P. Jiang, L. Chen, F. P. Yuan, and Y. T. Zhu, Proc. Natl. Acad. Sci. U. S. A. **111**, 7197–7201 (2014).

[28]X. L. Wu, M. X. Yang, R. G. Li, P. Jiang, F. P. Yuan, Y. D. Wang, Y. T. Zhu, and Y. G. Wei, Sci. China Mater. **64**, 1534–1544 (2021).

[29]C. X. Huang, Y. F. Wang, X. L. Ma, S. Yin, H. W. Hoeppel, M. Goeken, X. L. Wu, H. J. Gao, and Y. T. Zhu, Mater. Today **21**, 713–719 (2018).

[30]H. Zhou, C. X. Huang, X. C. Sha, L. R. Xiao, X. L. Ma, H. W. Hoeppel, M. Goeken, X. L. Wu, K. Ameyama, X. D. Han, and Y. T. Zhu, Mater. Res. Lett. **7**, 376–382 (2019).

[31]X. Y. Li, L. Lu, J. G. Li, X. Zhang, and H. J. Gao, Nat. Rev. Mater. **5**, 706–723 (2020).

[32]J. G. Li, Q. Zhang, R. R. Huang, X. Y. Li, and H. J. Gao, Scr. Mater. **186**, 304–311 (2020).

[33]Y. T. Zhu, K. Ameyama, P. M. Anderson, I. J. Beyerlein, H. J. Gao, H. S. Kim, E. Lavernia, S. Mathaudhu, H. Mughrabi, R. O. Ritchie, N. Tsuji, X. Y. Zhang, and X. L. Wu, Mater. Res. Lett. **9**, 1–31 (2021).